Strain ratio and thickness effects on plasticity and crack patterns of Nickel thin films

P. Godard, A. Guillot, F. Zighem, D. Thiaudière, D. Faurie, P.O. Renault

Version of Record: https://www.sciencedirect.com/science/article/pii/S1359646222001385
Manuscript_371f454410d07b62bd18ed2697a4baf8

Strain ratio and thickness effects on plasticity and crack patterns of Nickel thin films

P. Godard[a,*], A. Guillot[a], F. Zighem[b], D. Thiaudière[c], D. Faurie[b], P.O. Renault[a]

[a] *Université de Poitiers - CNRS - ENSMA, Futuroscope Chasseneuil, France*
[b] *LSPM - CNRS, Université Paris13, Université Sorbonne Paris Cité, Villetaneuse, France*
[c] *Synchrotron SOLEIL, L'Orme des Merisiers, Saint-Aubin, Gif-sur-Yvette Cedex, France*

Abstract

The influence of the strain ratio (equibiaxial or uniaxial) and the strain path (equibiaxial or sequenced uniaxial) on the cracking of metallic thin films is studied. We used 20, 100 and 600 nm Nickel films deposited onto flexible substrates, analysed with in-situ X-ray diffraction and digital image correlation, and post-mortem optical microscopy. It is shown that the thickness and the loading ratio effects are interweaved. In particular, 600 nm films show a small (1.9%) von Mises fracture strain and straight cracks when strained equibiaxially, but a larger (2.7%) fracture strain and more tortuous cracks when strained uniaxially. On the contrary, 20 and 100 nm thin films show different von Mises ultimate tensile strengths, though their von Mises fracture strain and theirs cracks tortuosity hardly depend on the test.

Keywords: Thin films; Fracture; Strain Path Change; X-ray diffraction; Crack pattern

Compliant electronic systems mainly rely on metallic thin films deposited onto stretchable polymers [1, 2, 3, 4]. Since the device lifetime depends on the integrity of the thin film, many studies have focused on the delamination or cracking of these films [5, 6, 7, 8]. In particular, thickness effects have been reported. However, most of these articles were restricted to uniaxial tests [9, 10, 11, 12, 13, 14]. Biaxial tests [15] or comparisons between uniaxial and biaxial tests [16, 17, 18, 19] are still scarce. This is nevertheless of paramount importance, since the device operating conditions lead to different loading or strain paths. In this article, we scrutinize the mechanical behaviours of Nickel thin films strained either equibiaxially or along a sequenced uniaxial test for a large range of thicknesses: 20, 100 and 600 nm, figure 1a. Noteworthy, each sequenced uniaxial test contains two uniaxial tests: one with the original microstructure, to be compared with the biaxial test, and one with films having long cracks (induced by the first loading) orthogonal to the second loading direction.

The Ni films were prepared by 1.2 keV Ar^+ ion beam sputtering in a Nordiko Hampshire-3000 Kaufman source, at a growing rate of 0.05 nm.s^{-1}; other details may be found in [17]. The films were deposited (simultaneously for the same thickness) on 25 μm thick Kapton®. The residual stress was equibiaxial and between -0.2 and -0.3 GPa, independent of the film thickness. The films were {111} fibre-textured, with full-width at half maximum (FWHM) of 20° for the thinnest sample, 12° for the other ones. Along the pole direction, the FWHM of the Bragg peaks are 0.52, 0.26 and 0.22° for the 20, 100 and 600 nm thin films, respectively.

A picture of the specimen mounted on the biaxial tensile tester is shown in figure 1b. This tensile tester, presented in [20], is available at the DiffAbs beamline of the synchrotron radiation facility SOLEIL. The cruciform stretchable substrates have 20 mm arm width and 90 mm length; the diameter of the disk-shaped thin films is 20 mm. Before the deformation test *per se*, an equibiaxial initial load of 4 N was applied. Optical images of the substrate rear surface are obtained with a telecentric lens and a charge-coupled device camera installed inside the machine; they allow in-plane true strain measurements thanks to a Digital Image Correlation (DIC) analysis (*Correli-q4* software [21]). Noteworthy, we showed in [22] that the strain is fully transmitted through the Kapton® substrate-Nickel film interface. Hence, the in-plane true strain components of the films are directly given by the DIC results. Examples of the in-plane true strain components applied to the specimen are given in figure 1c. A uniaxial strain test (UST) is followed, after 9%, by another uniaxial test in the orthogonal direction. This whole test is termed a sequenced uniaxial strain test (SUST, equivalent to the complex test in [17]); it is compared to an equibiaxial strain test (EBST) for which the two in-plane macroscopic strain components ϵ_1 and ϵ_2 are equally increased up to 9%. The other samples were similarly strained, but with slightly lower values: $6 - 8.5\%$. Note that, thanks to the biaxial machine, the UST we present are uniaxial in strain and not in stress, so that no buckles arise in the transverse direction.

Elastic strains were measured with *in-situ* X-Ray Diffraction (XRD) measurements, performed with a 250×300 μm^2 (vertical times horizontal) beam of energy 16.00 keV. The incident angle being 9°, the footprint

*Corresponding author. SP2MI - Téléport 2, 11 Boulevard Marie et Pierre Curie, BP 30179, F86962 Futuroscope Chasseneuil Cedex, France, Email address: pierre.godard@univ-poitiers.fr

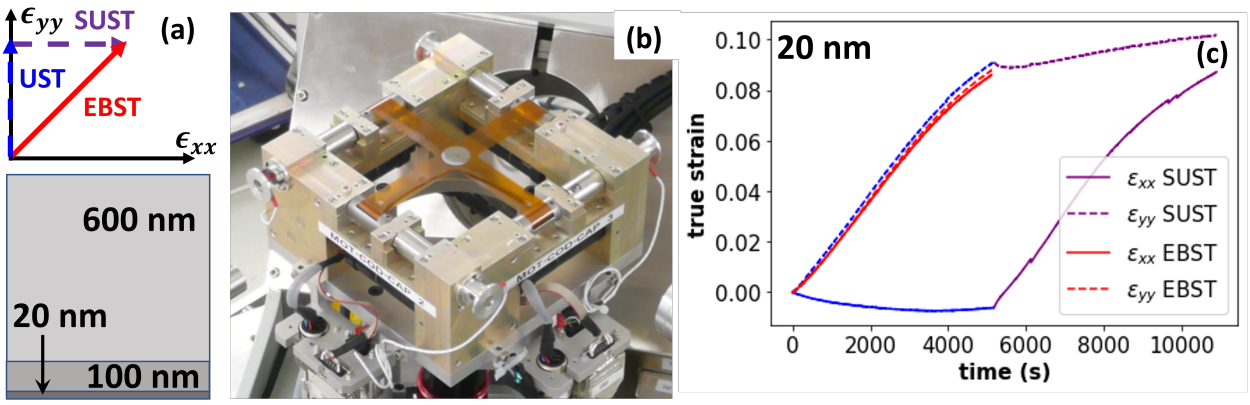

Figure 1: (a) The three mechanical tests (Equi-Biaxial, Uniaxial, Sequenced Uniaxial Strain Tests) and the three thicknesses studied in the article. (b) Picture of the biaxial tensile tester available at the DiffAbs beamline. (c) True strains for the 20 nm sample. The first parts of the SUST are represented in blue because they constitute the UST.

spread to 1600×300 μm^2, insuring a very good representativity of the XRD results. A two-dimensional detector (Mar 165-SX) lying 264 mm from the sample recorded images with an acquisition time of 5 (resp. 2, 1) seconds for the 20 nm (resp. 100, 600 nm) sample. The tensile tester was rotated by 90° between each image to capture both in-plane elastic strain components, ε_{xx} and ε_{yy}. The latter were determined through the classical $\varepsilon - \sin^2\psi$ method where ψ is the declination angle, *i.e.* the angle between the film surface normal and the scattering vector. The detector recorded portions of Debye-Scherrer rings corresponding to a range of ψ from 2 to 55°, or from $\sin^2\psi = 0.001$ to $\sin^2\psi = 0.67$. The linear $\varepsilon - \sin^2\psi$ curves were then extrapolated to $\psi = 90°$ to determine ε_{xx} and ε_{yy}, and to $\psi = 0°$ for ε_{zz}. Once the elastic strain tensor is known, the stress is determined *via* the Hooke's law with a Young modulus of 237 GPa and a Poisson ratio of 0.287 for the (111) planes, as determined with the Neerfeld-Hill model [22].

Figure 2 shows the two in-plane stress components as functions of time. One sees that the 20 nm sample is brittle: there are almost no transition between the elastic regime and the elastic relaxation induced by cracking. This is especially remarkable for the equibiaxially strained film, something we will return to later. For the 100 nm thin film, and even more for the 600 nm thin film, the stress components lose their linearity due to plasticity occurring in the film. The mechanical resistance of the sample decreases with its thickness, as expected [23]. In SUST, we observe that the larger the thickness, the smaller the ultimate strength of the second part of the test with respect to the one of the first part: indeed, for the 20, 100 and 600 nm films, the ultimate strength is 2.0, 1.5 and 1.4 GPa during the first straining test, respectively, and 2.1, 1.4 and 1.2 GPa when the film is stretched along the orthogonal direction. However, this effect is weak; in other words, cracks along the straining direction do not have a large effect on the load a thin film can support.

One also notes that because the Poisson ratio of the substrate is larger than the one of the film, a uniaxial strain test leads to tensile transverse stress in the film. One observes that cracks relaxes both stress components, the one along the strain direction and the transverse one. Another noteworthy point is that the stress relaxation is smoother for the 100 nm sample (though a small sliding in the grips happened in the EBST at 2300 s) than for the other ones. This is explained by two effects: first, the 20 nm thin film has the lowest scattering intensity since this is proportional to the illuminated volume; this accounts for the noise for this sample. Second, and more interestingly, the 600 nm sample (that has the data with the better signal over noise ratio) has cracks that are much more separated (because the distance between cracks increases with the film thickness, see below). The sudden stress jumps (e.g. arrows in figure 2c) is hence explained by the sudden propagation of one or two cracks in the diffracting volume (i.e. in the irradiated X-ray area of the film) - see also [24].

In order to pursue the comparison between the different mechanical tests, we plot in figure 3 the von Mises true stress as a function of the von Mises true strain. For clarity, we show only the first part of the SUST, corresponding to the UST. First, one observes that the slopes in the elastic regime are equal for the three thicknesses. Then, the mechanical resistance mentioned above is well evidenced and illustrates once again the well-known "smaller is stronger" effect [25]. A more innovative point is that this figure shows that the 20 and 100 nm samples have a higher strength in EBST than in UST, whereas these are equal for the 600 nm, but with a smaller plastic regime in the EBST. As already observed in uniaxial tensile tests [9, 10, 12], crack propagation appears at higher strain when the thickness of the film decreases. Here, the von Mises fracture strain, taken to be the von Mises strain at the

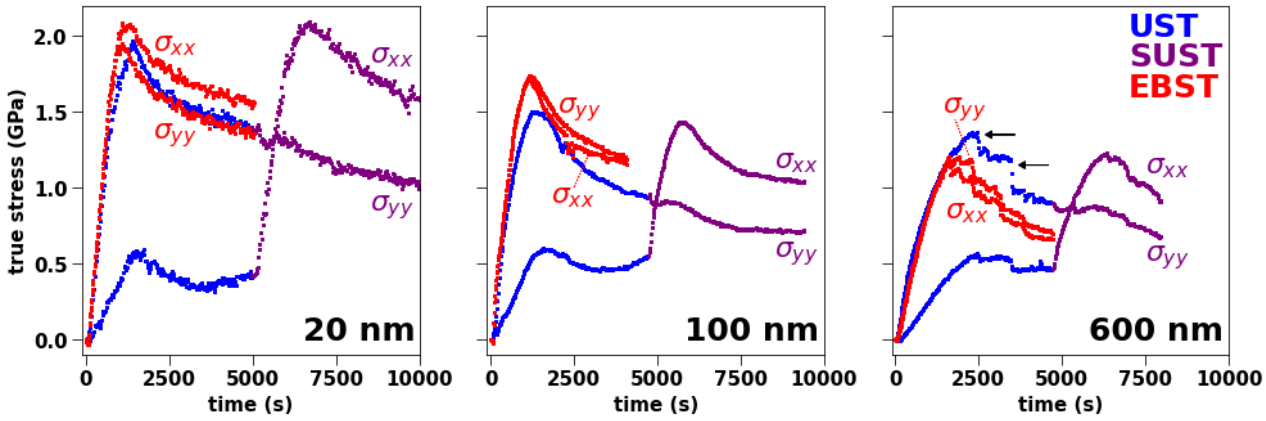

Figure 2: Stress components for several sample thicknesses and mechanical tests. The legend and scales are identical for all subfigures. The arrows for the 600 nm sample point to sudden jumps.

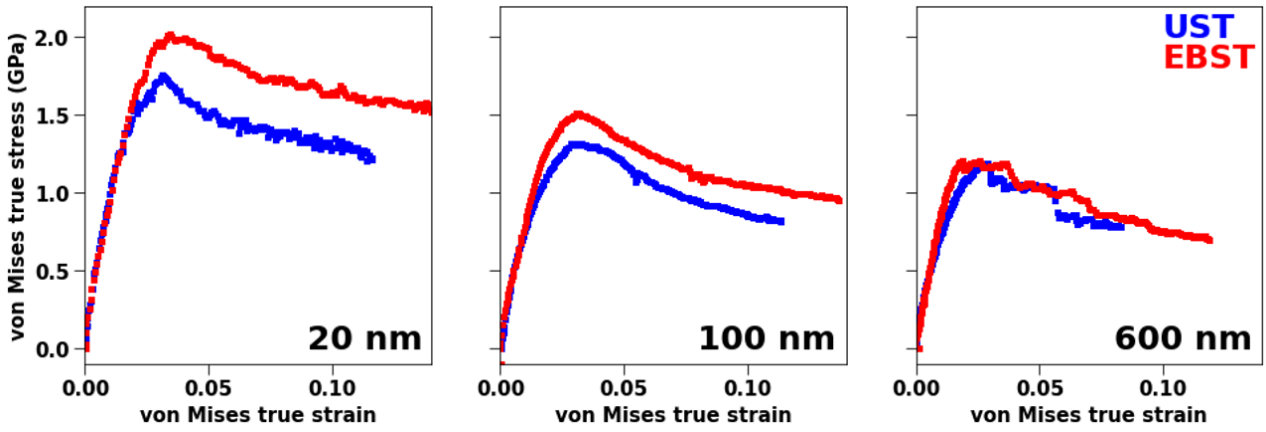

Figure 3: Applied von Mises true stress as a function of von Mises true strain, for equibiaxial (EBST) and uniaxial strain (UST) tests.

maximum von Mises stress, are 3.1, 2.9 and 2.7% in UST for 20, 100 and 600 nm films, and 3.4, 3.1 and 1.9% in EBST. That the thickest film has a much larger fracture strain in UST than in EBST shows again that the duration of the plastic regime is much shorter in equibiaxial tests. Since the residual stress values were similar for all samples, this behaviour is an extrinsic effect, and not an intrinsic one.

These ultimate tensile strengths, that appeared in components in figure 2 or in their von Mises equivalent in Figure 3, may surprise: they are associated here to cracking, and so to the brittleness of materials. Bulk brittle materials are characterized with a Rankine criterion: cracks appear when the maximum of a normal stress reaches a material-dependent threshold. This maximum stress criterion means that the two stress components lie within a square in the $(\sigma_{xx}, \sigma_{yy})$ plane, and the von Mises stress at a corner (corresponding to EBST) is equal to the von Mises stress at the middle of an edge (UST). Figure 3 shows that, for the 20 and 100 nm films, the von Mises ultimate tensile strength is larger in EBST than in UST, while figure 2 shows that the Rankine criterion is not satisfied either, since the ultimate tensile strengths do not coincide in UST and in EBST. Let us note nevertheless that the failure of composites is a complex multi-stage process. It is only once cracks have propagated beyond a certain extent, that the decreases of stress component values are captured.

Finally, we characterized the crack patterns through post-mortem optical images with a Keyence confocal microscope, figure 4a. As expected, EBST lead to mud crack patterns, whereas SUST give rectangular patterns, with presumably long cracks (horizontal direction in figure 4a) nucleated during the UST and small cracks nucleated in the transverse direction during the second part of the SUST. It is observed that the second set of cracks often crosses the first set. In the figure, the scale bar is chosen to be proportional to the sample thickness; that the subfigures, for a given test, display similar crack density shows that the latter is approximately proportional to the film thickness. This is evidenced quantitatively in figure

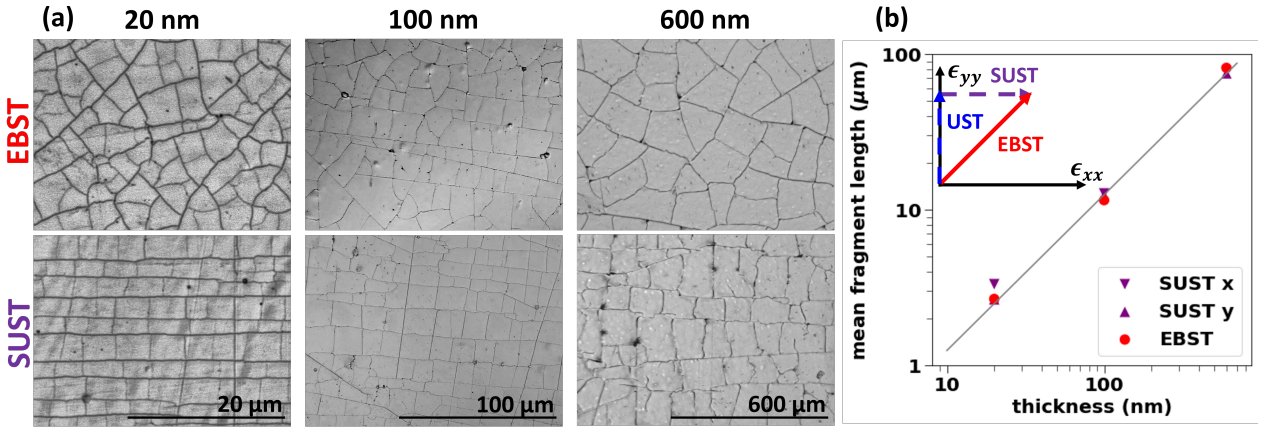

Figure 4: (a) Post-mortem optical images of the films. Top: mud crack patterns are observed for EBST. Bottom: rectangular patterns are obtained for SUST. The thinner samples show straight cracks, whereas the thicker are tortuous. The scale bars are proportional to the sample thickness. (b): Mean fragment length as a function of film thickness for UST, SUST and EBST. The directions were as isotropic as possible for the EBST. The schematics recall the straining directions.

4b, where we see that the mean fragment length l between cracks is 125 times the sample thickness h: $l \approx 125h$. Our estimation of l comes from a computation of a dozen of intercepts of cracks with a line of 50, 250 or 1000 μm, depending on the sample thickness; the resulting precision is about 10%. It is remarkable how these values are close for both parts of the SUST and the EBST, despite the fact that crack interactions depend on their respective orientations [26]. Let us nevertheless mention that this linear law differs from [11], where a fit $l = ah^n$, with $n \approx 0.5$ was found for uniaxial tests of Tantalum on Kapton®.

The relative brittleness of the thinner sample as compared to the thicker is once again evidenced: the thinner the film, the straighter the cracks. Moreover, the von Mises fracture strains obtained from X-ray diffraction analysis showed that the plastic regime extension is almost independent of the strain ratio for 20 and 100 nm films, but is larger in UST than in EBST for 600 nm films. This is well correlated with the sinuosity of the cracks observed in figure 4a: in the thicker film, the uniaxial strain test led to winding cracks, but equibiaxial test led to straight crack segments. Finally, we note that, in this sample, the vertical cracks seem to be more sinuous than the horizontal ones; this may come from the heterogeneous stress field lying in the sample when the vertical cracks appeared (the horizontal cracks appeared during the UST).

In conclusion, the unique biaxial device available at DiffAbs beamline allows comparisons between uniaxial (UST) and equibiaxial (EBST) strain tests on metallic thin films supported on compliant substrates. The thinner samples (20 and 100 nm thick) are stronger in EBST than in UST, while the 600 nm sample shows equal mechanical resistance (figure 3). The biaxial device also allows comparisons, without unloading the specimen, between pristine samples and transversally cracked samples when UST are opposed to sequenced uniaxial (SUST) strain tests. The ultimate tensile strength are then similar. Moreover, the stress-strain curves show that the plastic regime is slightly larger in uniaxial tests than in equibiaxial tests for 20 and 100 nm films (von Mises strain at maximum von Mises stress of 3.1 and 2.9 in UST versus 3.4 and 3.1 in EBST). This effect is more pronounced for the 600 nm film (2.7% versus 1.9%), and this is corroborated with the cracks sinuosity. Finally, though the crack patterns strongly depend on the strain ratio and the strain path, the mean crack spacing l depends only on the sample thickness.

Acknowledgements

The authors gratefully acknowledge SOLEIL for beam time allocation and Tarik Sadat for help during the experiments. This works was partially funded by the French Government programs “Investissement d’Avenir” (LABEX INTERACTIFS, reference ANR-11-LABX-0017-01, EUR INTREE, reference ANR-18-EURE-0010, JCJC PtyMet, reference ANR-19-CE08-0007).

References

[1] M. J. Cordill, O. Glushko, B. Putz, Front. Mater. 3 (2016) 11.
[2] D. Makarov, M. Melzer, D. Karnaushenko, O. G. Schmidt, Appl. Phys. Rev. 3 (2016) 011101.
[3] M. Melzer, D. Makarov, O. G. Schmidt, J. Phys. D: Appl. Phys. 53 (2020) 083002.
[4] F. Zighem, D. Faurie, J. Phys: Condens. Matter 33 (2021) 233002.
[5] K. Wu, J. Zhang, G. Liu, P. Zhang, P. Cheng, J. Li, G. Zhang, J. Sun, Acta Mater 61 (2013) 7889–7903.
[6] F. F. Schlich, A. Wyss, H. Galinski, R. Spolenak, Acta Mater. 126 (2017) 264–271.
[7] M. V. T. da Costa, J. Bolinsson, R. C. Neagu, P. Fayet, E. K. Gamstedt, Surf. Coat. Technol. 370 (2019) 374–383.
[8] K. Wu, Y. Xia, H. Yuan, J. Zhang, G. Liu, J. Sun, Mater. Sci. Eng. A 744 (2019) 746–753.

[9] Y. Leterrier, J. Andersons, Y. Pitton, J.-A. E. Månson, J. Polym. Sci. B: Polym. Phys. 35 (1997) 1463–1472.
[10] S. Frank, U. A. Handge, S. Olliges, R. Spolenak, Acta Mater. 57 (2009) 1442–1453.
[11] S. Frank, P. A. Gruber, U. A. Handge, R. Spolenak, Acta Mater. 59 (2011) 5881–5892.
[12] T. Jrg, M. J. Cordill, R. Franz, C. Kirchlechner, D. M. Tbbens, J. Winkler, C. Mitterer, Mater. Sci. Eng. A 697 (2017) 17–23.
[13] I. B. Cheikh, G. Parry, D. Dalmas, R. Estevez, J. Marthelot, Int. J. Solids Struct. 180-181 (2019) 176–188.
[14] M. J. Cordill, T. Jrg, D. M. Tbbens, C. Mitterer, Scripta Mater. 202 (2021) 113994.
[15] M. J. Cordill, P. Kreiml, B. Putz, C. Mitterer, D. Thiaudière, C. Mocuta, P. O. Renault, Scr. Mater. 194 (2021) 113656.
[16] S. Djaziri, D. Faurie, P. O. Renault, E. Le Bourhis, P. Goudeau, G. Geandier, D. Thiaudière, Acta Mater. 61 (2013) 5067–5077.
[17] D. Faurie, F. Zighem, P. Godard, G. Parry, T. Sadat, D. Thiaudière, P. O. Renault, Acta Mater. 165 (2019) 177–182.
[18] P. Godard, D. Faurie, P. O. Renault, J. Appl. Phys. 127 (2020) 105103.
[19] J. Li, C. Li, L. Li, Q. Wang, Z. Wang, S. Wang, C. Sun, Int. J. Solids. Struct. 219-220 (2021) 51–62.
[20] G. Geandier, D. Thiaudière, R. N. Randriamazaoro, R. Chiron, S. Djaziri, B. Lamongie, Y. Diot, E. Le Bourhis, P. O. Renault, P. Goudeau, A. Bouaffad, O. Castelnau, D. Faurie, F. Hild, Rev Sci Instrum 81 (2010) 103903.
[21] G. Besnard, F. Hild, S. Roux, Exp Mech 46 (2006) 789–803.
[22] P. O. Renault, T. Sadat, P. Godard, W. He, P. Guerin, G. Geandier, N. Blanc, N. Boudet, P. Goudeau, Surf. Coat. Technol. 332 (2017) 351–357.
[23] G. Dehm, T. J. Balk, H. Edongu, E. Arzt, Microelectron. Eng. 70 (2003) 412–424.
[24] V. M. Marx, F. Toth, A. Wiesinger, J. Berger, C. Kirchlechner, M. J. Cordill, F. D. Fischer, F. G. Rammerstorfer, G. Dehm, Acta Mater. 89 (2015) 278–289.
[25] O. Kraft, P. A. Gruber, R. Mnig, D. Weygand, Annu. Rev. Mater. Res. 40 (2010) 293–317.
[26] Z. C. Xia, J. W. Hutchinson, J. Mech. Phys. Solids 48 (2000) 1107–1131.

Declaration of interests

☒ The authors declare that they have no known competing financial interests or personal relationships that could have appeared to influence the work reported in this paper.

☐The authors declare the following financial interests/personal relationships which may be considered as potential competing interests:

aphical Abstract